STRUCTURE OF MATTER
AND QUANTUM CHEMISTRY

Computer Study of Silicene Channel Structure Based on the Transport of Li$^+$

A. E. Galashev[a,b,]* and K. A. Ivanichkina[a,b]

[a] Institute of High-Temperature Electrochemistry, Ural Branch, Russian Academy of Sciences, Yekaterinburg, 620137 Russia
[b] Yeltsin Ural Federal University, Yekaterinburg, 620002 Russia
**e-mail: galashev@ihte.uran.ru*

Abstract—The motion of a lithium ion in a silicene channel on an Ag(111) substrate under the influence of an electric field is modeled via molecular dynamics. The walls of the silicene channel are formed by both perfect silicene and silicene filled with vacancy defects of different types, and the surface area of silicene generally grows as the Li$^+$ moves along the channel. It is shown that when silicene contains mono- and divacancies, the roughness of its surface is less than with perfect silicene or tri- and hexavacancies. A moving lithium ion is used as a probe to study the structure of the inner walls of the channel. Voronoi polyhedra are constructed around the positions of ions at different times. One feature of the distributions of polyhedron elements is a shortened spectrum of angular arrangements of geometric neighbors with angles θ formed by pairs of Si atoms and the center (corner vertex) of the polyhedron. This type of θ spectrum is explained by the constant proximity of Li$^+$ to one of the silicene sheets forming the channel.

INTRODUCTION

A high theoretical capacity of 4200 mA h/g puts silicon among the most promising anode materials for lithium-ion batteries (LIBs) [1]. The most common anode material today is graphite, which has a capacity of 372 mA h/g. Silicon anodes can be damaged during lithiation and delithiation, and the contact between the active material and the current collector can disappear, making a battery unusable [2]. The new two-dimensional silicon material silicene is much more resistant to the cyclic stresses associated with lithium intercalation and deintercalation. The capacity of two-layer silicene (1384 mA h/g) is less than that of crystalline silicon (c-Si), but still notably higher than that of graphite [3]. In the future, we can expect the use of multilayer silicene as an anode material [4]. Multilayer silicene is obtained through the large-scale synthesis of silicene via liquid-phase oxidation and exfoliation of CaSi$_2$ [5]. A transmission electron microscope (TEM) shows that silicene has several layers retaining their original structure even after 1800 charging cycles.

Silicene was first obtained on a silver substrate. Today, it is most often deposited on an Ag(111) substrate [6, 7], with which it interacts strongly [8]. The energy of adhesion between them is 0.585 eV [9]. Silicene obtained in this manner is corrugated with a buckle size of ~0.74 Å [10]. A buffer layer of single-layer SiO$_2$ was created in [7] to weaken silicene interaction with the silver substrate. The high buckles in silicene and its strong bond with the metal substrate, reduce the filling of the silicene channel with lithium [11, 12]. The state of the surface of a channel wall is important for Li$^+$ to penetrate into the canal and subsequently move along the canal under the influence of an electric field. The nature of the movement of the ions affects the filling of the anode silicene channel with lithium, and thus the capacity of the anode and the battery as a whole.

The aim of this work was to study the structure of the walls of a silicene channel as a lithium ion moved along it.

COMPUTER MODEL

Two-layer silicene with an increased gap served as our channel for lithium intercalation. Each silicene sheet contained 300 atoms. The atoms in the lower silicene layer were exactly under the center of the regular hexagons belonging to the upper layer. The average distance between the nearest Si atoms in the same silicon sheet was 0.233 nm. Eight crystal planes of the silver fcc lattice were used as a substrate. As with two-layer silicene, the packing order of the Ag(111) planes was found to be ABAB. The interaction between Si

atoms in the same silicene sheet was created using the Tersoff potential [13]. The potential of an embedded atom (EAM) was used to describe the interaction between metal atoms in the substrate [14]. Cross interactions, including those between Si atoms belonging to different silicene sheets, were created using the Morse potential [15−17]. Calculations were made for a temperature of 300 K. Ag atoms interacted with Si atoms and Li$^+$ ions, but did not participate in thermal motion. This allowed us to more accurately reflect the macroscopic Ag(111) substrate, since the model used no periodic boundary conditions (PBCs). The immobility of Ag atoms did not introduce any strong distortions into the modeling results [8]. The absence of PBCs allowed us to trace the movement of Li$^+$ in the channel during its drift under the action of an electric field.

The unit cell of silicene had a rhombic shape and contained 18 atoms, six of which were elevated relative to the basal plane [18]. The silicene sheets were oriented relative to one another so that protrusions on their surfaces were directed outward. Calculations were made for the gap between silicene sheets: $h_g = 0.75$ nm. This allowed us to fill the silicene channel with lithium and was used to study the intercalation/deintercalation of lithium in the channel on metal substrates [1, 2, 19]. In this work, the initial distance between the lower silicene layer and the upper layer of the Ag(111) substrate was 0.247 nm, which corresponded to the DFT calculation [20]. The channel had no material side walls, but it was surrounded by an artificial force field that impeded the escape of atoms through the side and rear surfaces [19].

Li$^+$ was introduced into the channel through its entrance (front surface). Ions were drawn into the channel due to an applied electric field with a strength of 10^3 V/m. The period of residence for an ion in the channel was 150 ps or 1.5 million time steps ($\Delta t = 0.1$ fs). The channel walls were sheets of silicene that were either perfect or contained defects. The leaf size was 4.8 × 4.1 nm. Nine defects were distributed approximately evenly on each of the silicene sheets. Mono-, di-, tri-, and hexavacancies served as defects. A moving Li$^+$ ion was used as a probe to determine the structure of the inner walls of the channel. At each 10000 time steps (1 ps), a Voronoi polyhedron (VP) was constructed around the center of the ion. Si atoms in this case served as geometric neighbors of the ion. The procedure for constructing such (hybrid) VPs was described in [21, 22].

In this work, we used the standard LAMMPS code for molecular dynamics (MD) modeling [23]. Calculations were made on the URAN hybrid cluster computer at the Institute of Mathematics and Mechanics UB RAS with a peak performance of 216 Tflop/s and 1864 CPUs.

RESULTS AND DISCUSSION

The system configuration obtained after a 150 ps drift of Li$^+$ along the silicene channel is reflected in Fig. 1. Each sheet of silicene contained nine divacancies. As can be seen from the figure, both the upper and lower silicene sheets acquired the shape of a low dome with convexity directed upward. Only individual Si atoms in both sheets were displaced appreciably, and only two of them were detached from the top sheet. The considerable distortion of silicene sheets was due not only to strong interaction with the substrate but to their relatively small size as well. The distortion of the sheets after 150 ps is reflected in the area S their surfaces. Area S grew for almost all sheets of silicene as the Li$^+$ ion moved through the channel. An exception was the top sheet of silicene with monovacancies, where a very slight (0.3%) reduction in surface area was observed. The largest increase in S was observed for the lower sheets of silicene with hexavacancies (6.9%) and divacancies (6.3%).

The arithmetic mean of the absolute values of profile deviations or surface roughness was determined as

$$R_a = \frac{1}{n} \sum_{i=1}^{n} |z_i - \overline{z}|,$$

where z_i is the current z coordinate of ith atom, and $\overline{z}$ denotes the mean z coordinates of n atoms.

Roughness R_a obtained for the upper and lower sheets of silicene reflects Fig. 2. The R_a values of the sheets are obviously determined not only by the corrugated shape of silicene but by their deformation as well. Silicene sheets containing vacancy defects are generally less rough than perfect silicene sheets. An exception is channel walls that have trivacancies. The structure of these silicene sheets suffered the most destruction. The lower roughness of silicene sheets with mono- and divacancies was due to a reduction in the number of interatomic bonds and greater compliance that relieved the stress state, compared to sheets of perfect silicene. As a result, the global deformation of the sheets in these cases was not so great. The emergence of Si atoms detached from the channel walls when there were trivacancies in the sheets raised the value of R_a. The difference in the roughness values between the bottom and top sheets was greatest when there were hexavacancies in the silicene sheets. Since the bonds in this structure were on average, the weakest, the strong effect the Ag(111) substrate had on the state of the sheet's surface is clearly visible.
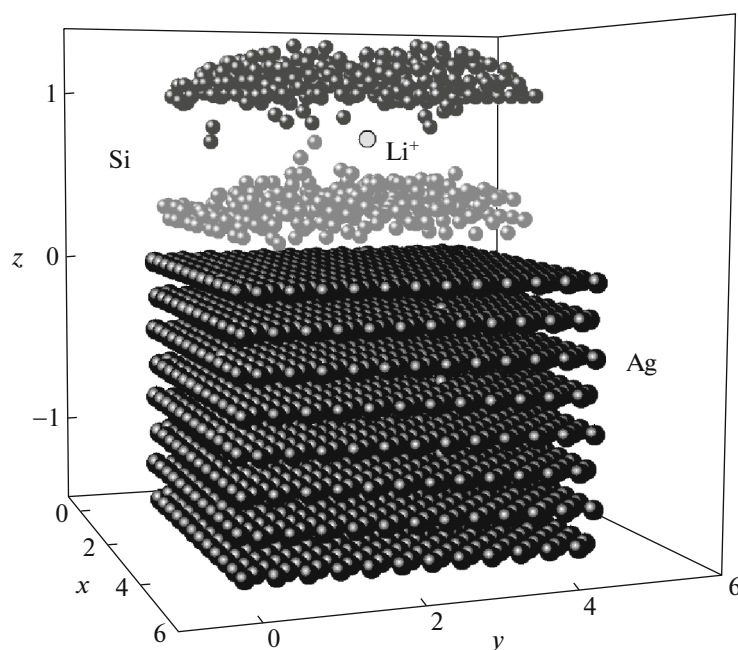
Fig. 1. Silicene channel on a Ag(111) substrate at the moment of 150 ps (Li$^+$ was in the channel the entire time). Each silicene sheet contains nine divacancies.

The calculated angular distributions of the nearest geometric neighbors for channels with walls of perfect and defective silicene are shown in Fig. 3. The main feature of these distributions is their shortened length. None of the distributions presented here have significant (nonzero) values at angles $\theta > 159°$. This could be due to the probe (Li$^+$) always being located near a channel wall. Due to the strong deformation of the channel walls and the height of the silicene buckles, the geometric Si neighbors of Li$^+$ that provide the faces of the VP basically belong to the same sheet to which the ion is attached. In other words, an VP built for an ion may not have a face formed from a Si atom belonging to the opposite sheet. The extra face from the Si atom of the opposite sheet is cut off from the VP by two or more faces obtained from Si atoms belonging to the ion-retaining sheet. Such a shortened θ-distribution is typical only of channels with metal substrates. A similar form of the θ distribution for channels on a graphite substrate yields an angular distribution of up to $\theta = 180°$, since an ion can be in the middle of the channel between the silicene sheets [24]. The adhesion of silicene to a graphite substrate is much weaker than to a metal substrate. The experimentally established energy of adhesion between graphene and silicon is 0.047 eV [25].

Nonzero values of the VP distribution over the number of faces (n-distributions) can range from $n = 9$ to 25 (Fig. 4). The largest standard deviation σ of this distribution is observed for the channel whose walls contain monovacancies caused by the n-spectrum having a nonzero value at $n = 25$. The lowest value of

σ is observed in the n-spectrum obtained for a channel whose walls contained hexavacancies. For a silicene channel with perfect walls, the value of σ is lower than for one with monovacancies, but more than for ones with all other types of defects. The maximum n-distribution falls most often on $n* = 16$. If the channel walls have monovacancies, however, $n* = 14$. If they have divacancies, $n* = 17$.
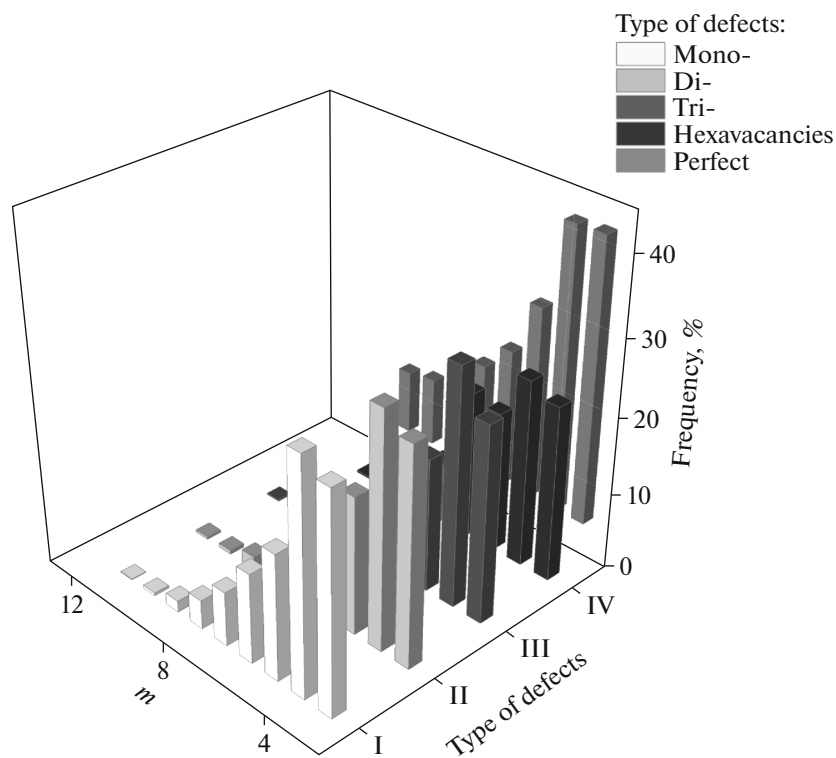
The distribution of VP faces according to number m of sides reflects the probabilities of observing
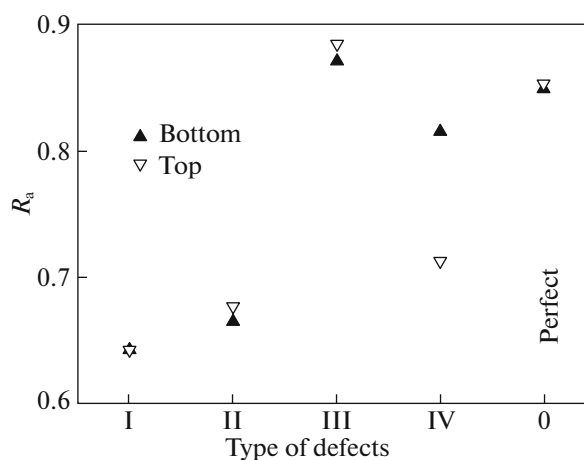

Fig. 2. Roughness of the bottom and top sheets of silicene at 150 ps; Roman numerals indicate the type of defects in the channel walls: (I) mono-, (II) di-, (III) tri-, (IV) hexavacancies.
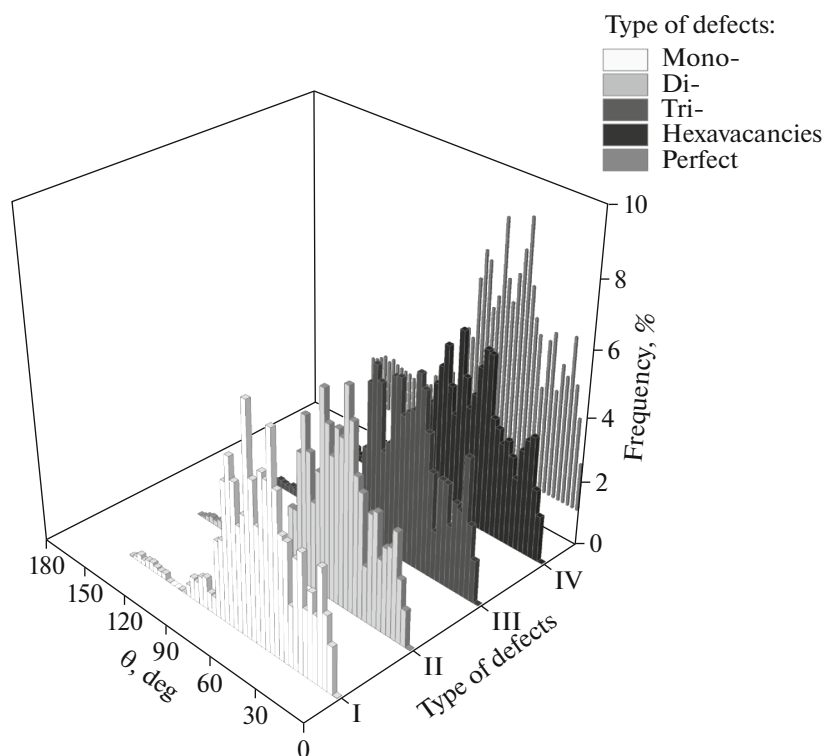
Fig. 3. Angular distributions of the nearest geometric neighbors for a silicene channel with walls containing defects: (I) mono-, (II) di-, (III) tri-, (IV) hexavacancies. The corresponding distribution for a channel made of perfect silicene is projected onto the rear coordinate plane.

Fig. 4. Distribution of VP according to the number of faces for a silicene channel whose walls contain defects: (I) mono-, (II) di-, (III) tri-, (IV) hexavacancies. The corresponding distribution for a channel made of perfect silicene is projected onto the rear coordinate plane.
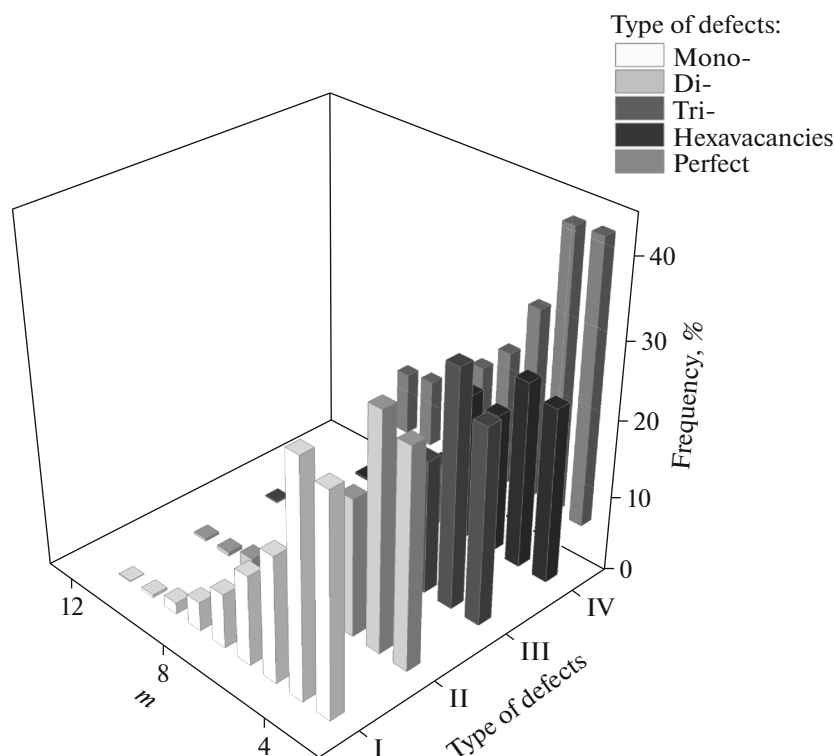
Fig. 5. Distribution of VP faces according to the number of sides for a silicene channel whose walls contain defects: (I) mono-, (II) di-, (III) tri-, (IV) hexavacancies. The corresponding distribution for a channel made of perfect silicene is projected onto the rear coordinate plane.

m-term cyclic formations from the center of an VP [26, 27], and the maxima of these distributions show the most probable rotational symmetry of the given system [28]. In the way described here for studying channel structure, m-term cyclic formations are created as a result of the close contact between Li$^+$ and Si atoms of any of the silicene sheets (Fig. 5). It should be noted that all of our m-distributions have a maximum at $m = 4$, most often from Li$^+$ directly in contact with four Si atoms. However, the frequency of five-membered formations emerging is also quite high for walls of perfect silicene, and only 0.5% lower than for formations with

$m = 4$. The importance of cyclic formations with $m = 5$ falls for silicene sheets with vacancy defects. The lag behind the number of formations with $m = 4$ can range from 25 to 46%. It is obvious that vacancy defects in silicene sheets reduces the number of the most likely close contacts between Li$^+$ and Si atoms.

CONCLUSIONS

Our study of the movement of Li$^+$ under the influence of an electric field showed that silicene channel walls can be deformed considerably, and in some cases even suffer minor damage. These results are mainly due to the strong effect a silver substrate has on the silicene sheets (channel walls). Together with the substantial atomic mass of silver and its high cost (relative to, e.g., graphite), this makes the use of such composites as anode materials for LIBs impractical. The high electrical conductivity of silver remains almost the only positive aspect of using the investigated composite material. It could be more promising for use in implantable electronics [29, 30].

Table 1. Areas of the upper and lower sheets of silicene (nm^2) at initial moment (I) and after a 150 ps drift of the lithium ion (II)

Defect	I		II	
	upper	lower	upper	lower
Perfect	18.572	18.578	18.7	18.631
Monovacancies	18.524	18.523	18.468	19.112
Divacancies	18.468	18.463	19.196	19.639
Trivacancies	18.448	18.447	18.809	18.823
Hexavacancies	18.013	18.326	18.996	19.589

REFERENCES

1. A. Y. Galashev and K. A. Ivanichkina, J. Electrochem. Soc. **165**, A1788 (2018).
2. A. Y. Galashev and K. A. Ivanichkina, ChemElectro-Chem **6**, 1525 (2019).
3. A. E. Galashev and K. A. Ivanichkina, J. Struct. Chem. **61**, 659 (2020).
4. J. J. Liu, Y. Yang, P. B. Lyu, et al., Adv. Mater. **30**, 1800838 (2018).
5. G. A. Tritsaris, E. Kaxiras, S. Meng, and E. G. Wang, Nano Lett. **13**, 2258 (2013).
6. B. Aufray, A. Kara, S. B. Vizzini, et al., Appl. Phys. Lett. **96**, 183102 (2010).
7. Y. Du, J. Zhuang, J. Wang, et al., Sci. Adv. **2**, e1600067 (2016).
8. A. Y. Galashev and K. A. Ivanichkina, Letters on Materials **9**, 270 (2019).
9. W. Wei, Y. Dai, and B. Huang, J. Mater. Chem. A **5**, 18128 (2017).
10. K. Kawahara, T. Shirasawa, R. Arafune, et al., Surf. Sci. **623**, 25 (2014).
11. A. Y. Galashev and K. A. Ivanichkina, Phys. Lett. A **381**, 3079 (2017).
12. A. Y. Galashev and K. A. Ivanichkina, J. Electrochem. Soc. **167**, 050510 (2020).
13. J. Tersoff, Phys. Rev. B **39**, 5566 (1989).
14. S. M. Foiles, M. I. Baskes, and M. S. Daw, Phys. Rev. B **33**, 7983 (1986).
15. R. Yu, P. Zhai, G. Li, and L. Liu, J. Electron. Mater. **41**, 1465 (2012).
16. K.-N. Chiang, C.-Y. Chou, C.-J. Wu, et al., ICCES **9**, 130 (2009).
17. S. K. Das, D. Roy, and S. Sengupta, J. Phys. F: Met. Phys. **7**, 5 (1977).
18. A. E. Galashev, O. R. Rakhmanova, and K. A. Ivanichkina, J. Struct. Chem. **59**, 877 (2018).
19. A. Y. Galashev and K. A. Ivanichkina, Phys. Chem. Chem. Phys. **21**, 12310 (2019).
20. Z. Qin, Z. Xu, and M. J. Buehler, J. Appl. Mech. **82**, 101003 (2015).
21. A. E. Galashev, O. R. Rakhmanova, and V. N. Chukanov, Colloid. J. **67**, 271 (2005).
22. A. N. Novruzov, O. R. Rakhmanova, and A. E. Galashev, Colloid. J. **70**, 55 (2008).
23. S. Plimpton, J. Comput. Phys. **117**, 1 (1995).
24. A. E. Galashev and K. A. Ivanichkina, Phys. Solid State **61**, 233 (2019).
25. Z. Zong, C.-L. Chen, M. R. Dokmeci, and K.-T. Wan, J. Appl. Phys. **107**, 026104 (2010).
26. A. E. Galashev, Colloid. J. **76**, 300 (2014).
27. A. E. Galashev, Phys. Met. Metallogr. **117**, 238 (2016).
28. A. E. Galashev, Russ. J. Phys. Chem. B **8**, 793 (2014).
29. D. H. Kim, J. Viventi, J. J. Amsden, et al., Nat. Mater. **9**, 511 (2010).
30. M. P. Stoykovich, J. Z. Song, V. Malyarchuk, et al., Nature (London, U.K.) **454** (7205), 748 (2008).